Effects of Distributed Electric Propulsion on the Performance of a General Aviation Aircraft

Murilo A. Gallani* and Luiz C. S. Góes, †
Instituto Tecnológico de Aeronáutica, São José dos Campos, São Paulo, Brazil

Luiz A. R. Nerosky‡
Embraer, São José dos Campos, São Paulo, Brazil

With an always increasing demand for more efficient aircraft due to both economic and environmental purposes, academy and industry are studying hybrid-electric and full-electric concepts to explore new aircraft design opportunities. This paper proposes a study based on a Cessna 208B Grand Caravan, using it as a platform to implement distributed electric propulsion and enable the use of high-lift propellers by electrifying the propulsive system. Key design parameters of the aircraft are varied to evaluate the effectiveness of the lift augmentation system as well as its effects on generated thrust and aerodynamic efficiency. The effects of the propellers slipstreams on the wing are implemented on SUAVE, a conceptual level design environment, which is used to integrate the aircraft model and run the simulations. Results of the analyses differ from what is available on the literature, yielding aerodynamic efficiency gains that are much more modest than what was expected according to assumptions made on recent publications.

I. Nomenclature

A	=	Propeller disk area
b	=	Wingspan
β	=	Ratio between actual and maximum theoretical K_L
c	=	Airfoil chord, wing section chord
$(cl)_\infty$	=	Wing section unblown lift coefficient
C_D	=	Drag coefficient
C_{D_0}	=	Drag polar constant term
C_{D_i}	=	Induced drag coefficient
C_{D_p}	=	Parasitic drag coefficient
C_L	=	Lift coefficient
$C_{L_{max}}$	=	Maximum lift coefficient
C_{L_∞}	=	Unblown lift coefficient
k	=	Drag polar lift dependent term
K_L	=	Ratio between blown and unblown lift coefficient
L/D	=	Lift to drag ratio (aerodynamic efficiency)
q_{ratio}	=	Dynamic pressure ratio
R	=	Propeller radius, half of slipstream height
ρ	=	Air density
S	=	Wing area
S_{aff}	=	Flap affected wing area
S_{blown}	=	Blown wing area
S_{ratio}	=	Modified wing area to reference aircraft wing area ratio
v_i	=	Propeller induced velocity
V_j	=	Jet velocity
V_p	=	Propeller induced velocity
V_∞	=	Freestream velocity

*M. Eng. Student, Divisão de Engenharia Aeronáutica
†Full Professor, Divisão de Engenharia Mecânica
‡Senior Manager, Research and Technology Department

II. Introduction

The aeronautical industry is currently researching and investing on the electrification of aircraft to reduce the overall mission fuel burn and lessen its emissions on the atmosphere and a number of new concepts and technologies are being developed and studied [1, 2] . Merely replacing fuel with batteries and electric energy or hybridizing conventional aircraft does not seem to bring clear benefits [3–5] unless really optimistic technology assumptions are used, specially on the battery side [6].

It is proposed that one of the main lines of research for new aircraft should be on aircraft-propulsion integration [7], seeking positive interactions between the propulsors and the airframe to increase flight efficiency. Electrification then can be used to explore new engine mount positions, distribute propulsors on different parts of the aircraft or trying completely new fuselage and wing forms and configurations to achieve more efficient flight.

That being said, the main objective of this paper is to evaluate, on a conceptual design level, the effects of distributed propulsion on the performance of a general aviation aircraft when using electric motors to enable the use of propellers as high-lift devices. These effects will be verified by studying a redesign of a Cessna 208B Grand Caravan, modifying its propulsive system and wing to accommodate the new concept and verifying how the aerodynamic efficiency of the aircraft changes as some key design parameters are varied.

III. Literature Review

One of the most promising applications of Distributed Electric Propulsion is its use to enable the concept called High Lift Propellers (HLP), which has been explored in many different publications [8–12]. This concept consists in distributing propulsive power and thrust through several relatively small propellers that are installed ahead of the leading edge of the wing with the purpose of blowing their slipstream on it during takeoff and landing, increasing the generated lift. An example of this concept can be seen in Figure 1. Concepts that use this technology use the high lift propellers only at low speed flight when higher values of lift coefficient are needed whereas during cruise, for instance, the concepts aim to turn off some or all of the HLP and fold back their blades to reduce drag.

Fig. 1 A concept aircraft using the HLP technology. [8]

The propellers increase the local dynamic pressure on the wing, increasing the total generated lift and increasing the $C_{L_{max}}$ that can be achieved. This increase in C_L is merely a translation of this increase in local dynamic pressure since the coefficient is calculated based on the freestream conditions. The wing area can then be reduced to increase the wing loading and, according to the L/D curve for a given drag polar, greatly increase aerodynamic efficiency [11, 12].

Figure 2 shows an example using an estimated drag polar of the Cirrus SR22 [12]. This curve was generated as a function of the wing loading and, assuming a constant cruise altitude and speed, it also directly relates to cruise C_L as higher wing loading values require a higher lift coefficient to fly. The figure also shows the stall speed curve as function of wing loading for a maximum lift coefficient of 2. Higher wing loading values mean that, to keep the aircraft aloft at this given C_L higher speeds are required and thus, higher stall speed values are reached.

The maximum stall speed allowed for this kind of aircraft according to FAR Part 23 is represented on the figure by the horizontal line at 61 knots, showing that there is a maximum possible wing loading that complies with this requirement, and it is not high enough to result in an optimal cruise L/D. In fact, the achieved lift-to-drag ratio is

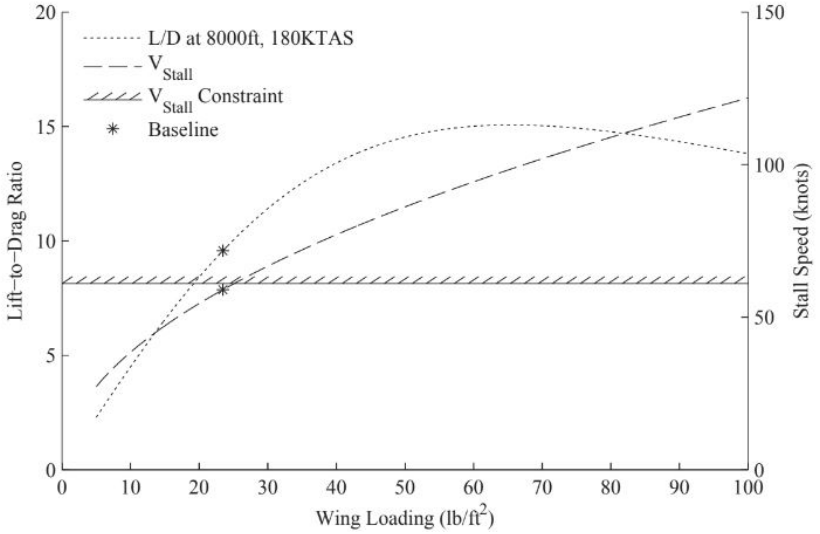

Fig. 2 Cirrus SR22 estimated cruise L/D versus design Wing Loading. [12]

around 33% smaller than the optimal which shows a potential gain of 50% in aerodynamic efficiency if flying at higher values of wing loading.

The effect is also shown in Figure 3 with cruise L/D plots at various speeds for a wing that was designed for a stall speed of 61 knots at sea level and four different maximum lift coefficient numbers. For low $C_{L_{max}}$ values the optimal cruise speed is fairly low, at around 110 knots for the case presented before of a $C_{L_{max}}$ of 2. As the maximum lift coefficient increases, reducing wing size and increasing the wing loading, the best L/D ratio happens at higher speeds, shifting the curves to the right.

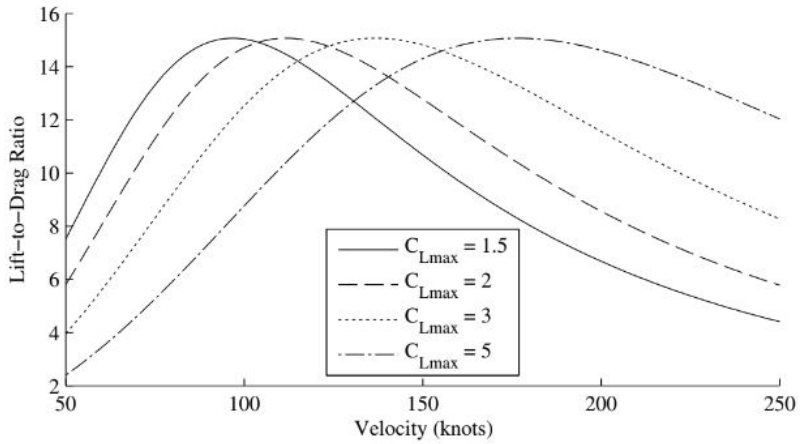

Fig. 3 Cirrus SR22 estimated L/D for different speeds and design $C_{l_{max}}$ [12]

There are some studies that try to quantify the advantages and feasibility of such configuration. Stoll *et al.*[8] show an L/D of over 20 for a concept aircraft that is similar in size to the Cirrus SR22. By using high-lift propellers the author manages to reduce wing area by 62%, increasing wing loading by 131%. On another study, Stoll [9] tries to verify the wing simulation results by comparing it to experimental data, and finds that the experimental and analytical results are off by only 10% according to preliminary analyses.

The results from these analyses look very promising, showing a lot of potential gains in using electrification to propel new concepts. This backs up the idea that the focus of research on new and more efficient aircraft should inevitably be

on Aircraft-Propulsion Integration, using the benefits of electrification and Hybrid-Electric Propulsion as enablers for new propulsive and aerodynamic concepts.

IV. Models

In this section the main models used in this work are be presented. To analyze the effects of high-lift propellers on the performance of an aircraft a few core models were implemented and integrated on a tool that will work as a mission solver to generate the results for analysis.

Stanford University Aeronautic Vehicle Environment (SUAVE) [13] is the mission solver of choice for this work. It was made specifically for conceptual level design with focus on studying unconventional and futuristic aircraft.

A. General Models

On SUAVE, an aircraft is built by linking together several components like wing, fuselage, landing gears, etc., each with its own performance methods and metrics. On the next paragraphs a brief explanation of each of the different component models used will take place.

For calculating the drag on wing-like surfaces and fuselage the methods already available in SUAVE [13] were used. The only change was on the fuselage drag, where the drag was increased based on the increased dynamic pressure of the nose propeller. A Vortex Lattice method for lift calculation is also available on the solver and was not changed for this work. The resulting C_L calculated by this method was then modified by Equation 4 based on the lift augmentation model that will be introduced later on this section. As for induced drag, a simple equation based on Oswald Efficiency Factor and wing aspect ratio is used.

The nacelles that hold the electric motors and high-lift propellers were considered to be streamlined structures, considerably smaller than traditional turboprop nacelles, so they were represented by the drag estimate equation for external fuel tanks presented by Gudmundsson [14] due to the similarities in shape and size. A fixed drag coefficient of 0.07 was considered for each nacelle, using as reference area its frontal section which is dictated by the motor diameter. A proprietary model [15] to estimate motor diameter based on power and angular speed was used to couple propeller power requirements and drag.

Flap drag was calculated based on the method proposed by Gudmundsson [14] with empirical equations that take into consideration flap type, chord, thickness, deflection and span. For the Grand Caravan, the equations for slotted flaps with a t/c of 0.12 was used. The flap lift was calculated based on available data from the Cessna Grand Caravan Information Manual [16].

The aircraft used in this study has non-retractable landing gears and also a strut supporting the wing that is connected on the fuselage, so these components drag also were calculated based on the methods found on Gudmundsson [14].

The drag equation for streamlined struts was used for the wing strut and the landing gear drag was calculated based on the predetermined drag coefficients of 0.615 for the main landing gear and 1.9 for the nose landing gear, using as reference area the estimated tire frontal area.

Excrescence drag was calculated with a method available on SUAVE, which is a simple polynomial equation that fits some of the data available on ESDU 94044. However, the value obtained with this polynomial was adjusted to calibrate the model drag polar and match it to the one of the real aircraft, as will be explained on further on this section.

B. Reference aircraft

The Cessna 208B Grand Caravan baseline model was created by estimating the original aircraft drag polar and then using the models presented to create an aircraft on SUAVE.

Data available on the Grand Caravan Information Manual [16] for cruise flight was used to estimate the baseline drag polar. C_L and C_D values were gathered for a wide range of conditions, using data from altitudes of 2000, 10000, 16000 and 20000 ft cruise flight. The calculations were based on the aircraft MTOW of 8750 lb (3969 kg) and wing reference area of 279 ft^2 (25.95 m^2). For the drag coefficient the shaft power was calculated at each point based on RPM and torque data and an assumption of 82% propeller efficiency, and then used to calculate thrust and thus drag. This process resulted on a drag polar of $0.03689 + 0.04606\ C_L^2$, shown in Figure 4.

Using the models presented earlier the aircraft was assembled on SUAVE and had its drag polar calibrated to match the data gathered from the Manual by adjusting the excrescence drag component. This was done by running the model on a calibration mission at several speeds and altitudes to collect C_L and C_D data and fit it to a two term equation just

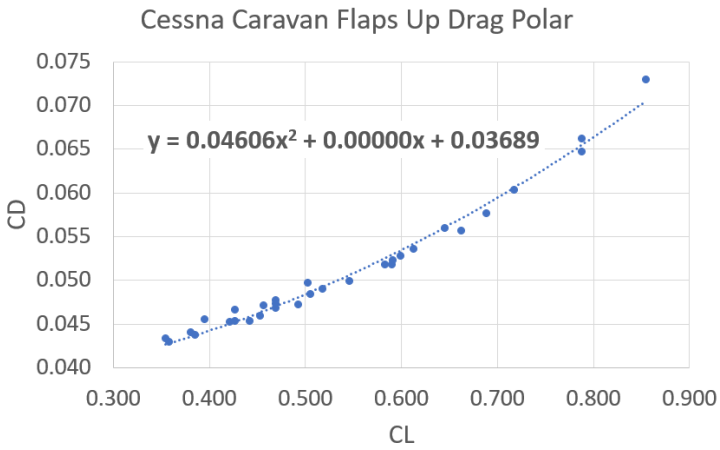

Fig. 4 Grand Caravan estimated drag polar.

like it was done with the real aircraft, adjusting the model until the polar matched the desired equation. The results can be seen on Figure 5, along with the calibration mission profile.

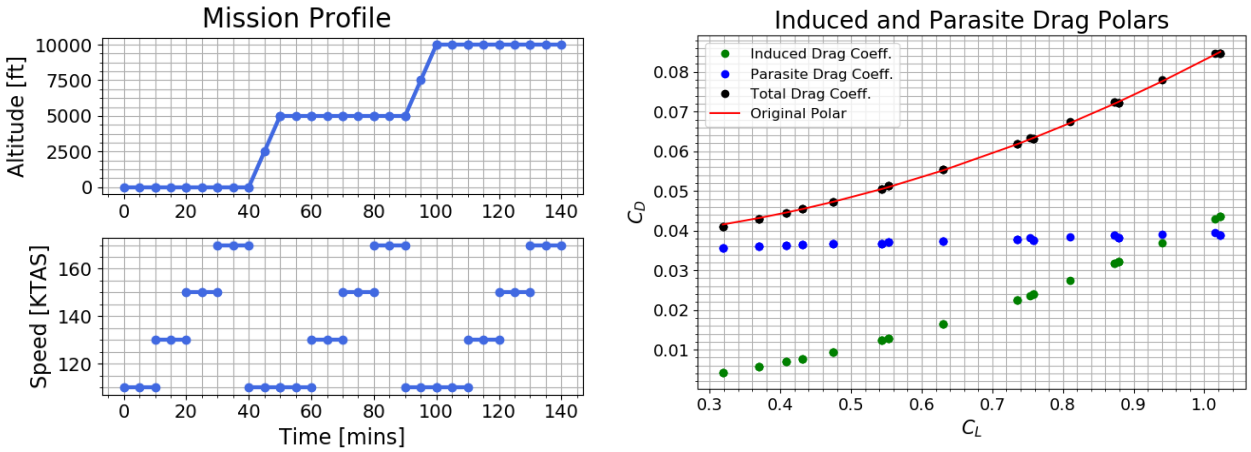

(a) Mission profile.

(b) Lift and drag data.

Fig. 5 Grand Caravan model aerodynamic calibration.

C. Hybrid-electric aircraft model

The modified hybrid-electric aircraft uses as a starting point the previously modeled Grand Caravan so all the aerodynamics are in large part unaltered on the new model. There are two notable differences that will be addressed on this section: propulsive system and wing changes.

The propulsive architecture of choice for this aircraft is a partial-turboelectric, as seen on Figure 6. On this system the turboprop engine remains exactly where it is on the conventional aircraft, powering the cruise propeller mechanically through a gearbox. Connected on the same shaft is a generator, so that the total shaft power delivered by the engine can be properly split between both components depending on the load on each one of them. The load on the propeller is modulated by the blade pitch while on the generator it is controlled by how much electric power is being demanded by the system. The power supplied by the generator is then distributed by cables to motor controllers that will in turn control and power the wing-mounted electric motors that drive the high-lift propellers.

The main driver for this choice was to minimize the impact in propulsive efficiency that the aircraft modifications will bring. By maintaining the original engine-propeller mechanical coupling during cruise no electrical losses take

place, maximizing efficiency during this flight phase. On the electrical side, the choice for a generator instead of a battery system was mainly due to the high weight of batteries given its low specific power and energy.

All these extra components were also modeled in terms of performance and weight, as explained on [15], however since this is not part of scope of this paper it will not be presented here.

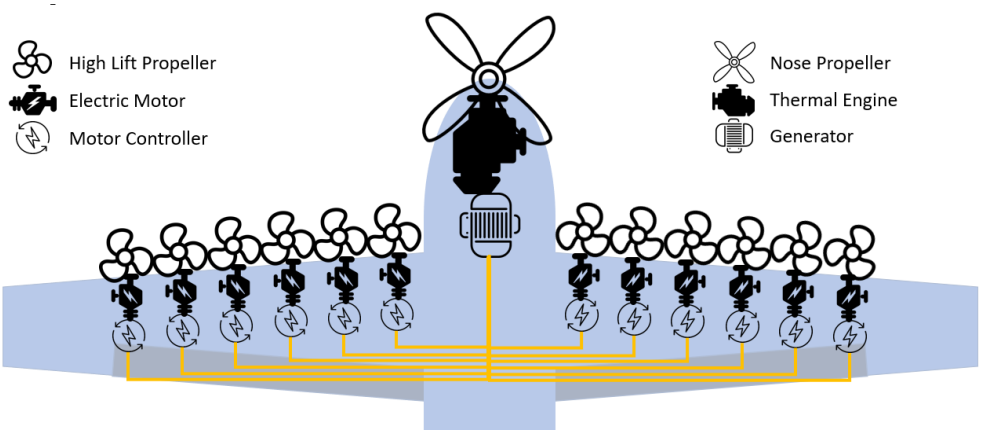

Fig. 6 Chosen propulsive architecture.

The wing is another component that changes dramatically on the new aircraft, specially it's reference area. Simplifications were be made to reduce the number of variables to be watched and to mitigate effects that are not related to the wing blowing effect.

One of the assumptions was to maintain many of the geometric aspects of the wing unchanged such as taper ratio, twist, sweep, etc. The reason behind this was to make sure that any variations in weight and drag would be the result of the addition of the DEP system and reduction in wing area and not simply better wing design. On this same line of thought, the aircraft Oswald efficiency factor and unblown $C_{L_{max}}$ were kept unchanged.

Another factor was the flap-affected area, S_{aff}, of the wing. To avoid worrying about resizing the flap and the subsequent effects in maximum lift coefficient, the ratio between S_{aff} and the wing reference area S_{ref} was kept constant. The same idea was applied to flap chord, keeping it proportional to the mean aerodynamic chord of the wing. Besides that, the blown area was chosen to be equal to the flap-affected area meaning that all the high lift propellers blow on flapped sections of the wing and are not too close to the wingtip.

Another assumption that affects not the wing itself, but the blowing effect, is that the propellers all have the same size and blow sections of the same chord, defined as the mean chord between the wing root chord and at the end of the blown area. This assumption was made to simplify the model, avoiding many different radius-to-chord ratio, propeller speeds, motor sizes, etc.

With these assumptions, many of the potential wing variables do not become variables at all during the analyses, and can be defined analytically based on other values. The main variable that is changed extensively on this study is the wing area, and that change is flowed down to other wing geometric parameters.

D. High-Lift Propellers

The main thing to be modeled for the HLP is the relationship between propeller size, thrust and slipstream velocity. The chosen method to model these propellers was the momentum theory, represented by Equations 1 and 2. They allow simple calculation of the generated thrust T or slipstream velocity v_i based on propeller disk area A, freestream velocity V_∞ and air density ρ without worrying with details of blade geometry. To estimate propeller efficiency data from a high-lift propeller design exploration study made by Patterson [12] was used and, on the design point, was around 64%.

$$T = \rho A \left(V_\infty + v_i\right) \left(2v_i\right) \tag{1}$$

$$v_i = \frac{-V_\infty + \sqrt{V_\infty^2 + \frac{2T}{\rho A}}}{2} \tag{2}$$

E. Lift Augmentation

The model used for the interaction between propeller and wing was replicated from Patterson [12]. It couples well with the momentum theory for propellers and is simple enough that allows for fast calculations without the need for expensive and time consuming CFD simulations.

The author starts with a very elementary case of a flat plate of length c immersed on a slipstream of height $2R$ that is on the same direction of the freestream, as is represented on Figure 7.

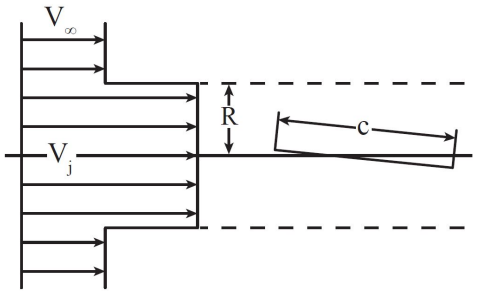

Fig. 7 Flat plate in a slipstream. [12]

Since in this configuration there is no change in the angle of attack due to the slipstream, the change in lift coefficient of the section is merely proportional to the change in dynamic pressure on the plate. So, if c_l is the lift coefficient of the plate on the slipstream and $(c_l)_\infty$ is the coefficient of the plate on the freestream alone, the multiplier K_L can be expressed by equation 3 where the jet velocity V_j is the sum of the freestream velocity V_∞ and the propeller induced velocity V_p.

$$K_L = \frac{c_l}{(c_l)_\infty} = \frac{V_j^2}{V_\infty^2} \tag{3}$$

This shows that the increase in lift coefficient in this particular case can be expected to raise linearly with the dynamic pressure or with the square of the velocity increase. However, a study from Ting and Kleinstein [17] shows that that is not always the case, and the lift increase K_L is affected by the ratio between the slipstream height R and the airfoil chord c as is shown in Figure 8a, where the theoretical increase is reached only for radius-to-chord ratios greater than one. The factor β is defined to represent the ratio between the achieved value of K_L and its theoretical maximum, shown in figure 8b.

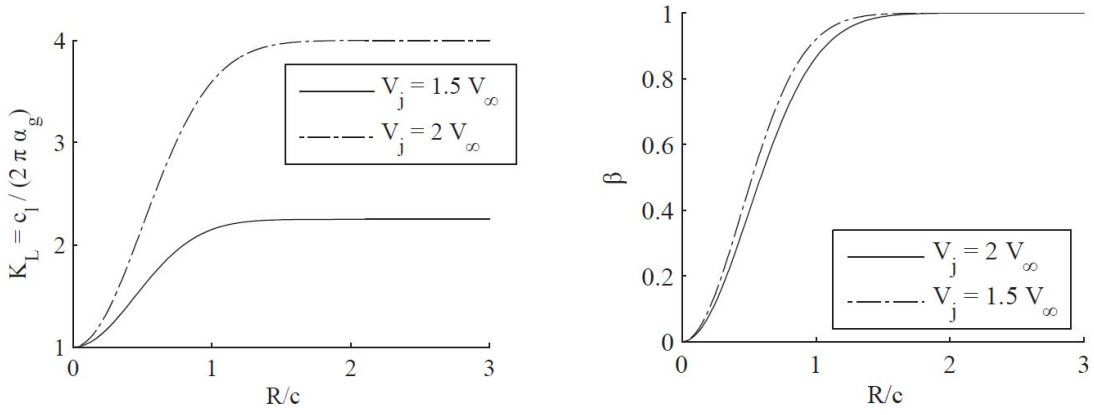

(a) Change in K_L with R/c ratio.

(b) Change in β with R/c ratio.

Fig. 8 Lift increase changes with R/c ratio. [12]

Patterson [12] develops a model for β based on a series of CFD simulations of a propeller disk of different radii R positioned upstream of a NACA 0012 airfoil of chord c. Besides changing the propeller radius the distance u from the propeller to the airfoil and its angle of attack are also varied, as well as the ratio between the slipstream and freestream velocities, to gather the data. The equations that result from this data and model the factor β can be found on the author's original work. For this paper it is enough to state that the model was replicated and implemented, and the final equation to calculate the lift coefficient on the wing was deduced.

With the assumption that all propellers blow an equal portion of wing area, with the same R/c and u/c ratios the whole wing lift coefficient can be easily calculated with the factor β and the blown area ratio based on a previously calculated C_{L_∞} for the unblown wing, represented by Equation 4 where in this case S_{blown} is the total area blown by the propellers.

$$C_L = C_{L_\infty}\left(1 + \frac{S_{blown}}{S}\left(\frac{(\beta V_p + V_\infty)^2}{V_\infty^2} - 1\right)\right) \tag{4}$$

V. Analyses and Results

Based on the original Grand Caravan estimated drag polar, its L/D curve as function of C_L is plotted on Figure 9. When flying at 10000 ft at a cruise speed of 168 kt the aircraft lift coefficient is 0.452 which yields a L/D of 9.84. This aircraft flies most efficiently at a C_L of 0.895 and L/D of 12.13, which would happen at 10000 ft if flying at a speed of 120 kt, trading speed for efficiency.

According to the studies and theory presented earlier, this shows that the aircraft has the potential to increase it's aerodynamic efficiency by approximately 23% if it could fly at a higher C_L, implicating in having a wing of approximately half the size of the current one. This gives an idea of the goal for the DEP system that will be implemented, attempting to double the maximum C_L to manage a wing of half the size without affecting it's stall speed.

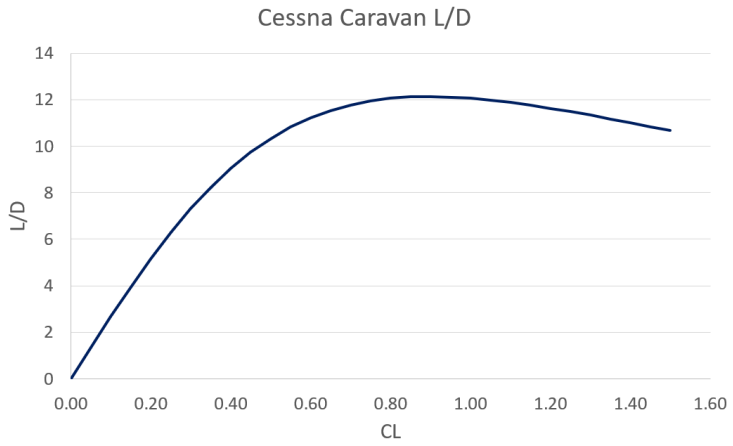

Fig. 9 Grand Caravan estimated aerodynamic efficiency curve.

The analysis presented here aims to observe and gather data on how the aircraft performance changes as the design space for the main variables is explored. Wing area ratio and propeller dynamic pressure ratio were swept over a range of values and the aircraft sized based on the previously discussed methods and assumptions, generating a number of subjects to be evaluated.

The number of high-lift propellers would also influence the results, as it affects their diameters and thus the lift augmentation and thrust generation capabilities. In the analyses presented in this paper there was no variation of this parameter and all the results were generated with a total of ten high-lift propellers, five on each semi-wing. A sensitivity study to find how the results change with the variation of this number can be found on [15].

Wingspan and aspect ratio were varied following two different approaches where each of these quantities was kept constant in turn while the other varied. When wingspan is kept constant, as the wing area is reduced the aspect ratio increases and wing chord is reduced and, if aspect ratio is kept constant, both the wingspan and wing chord are reduced.

Based on the assumptions presented in this paper, the design variables of the aircraft were reduced to three:

- S_{ratio}: Wing area ratio, which is the ratio between the new wing reference area S_{new} and the original S_{ref}.
- q_{ratio}: Dynamic pressure ratio, which is how much the the dynamic pressure q_{blown} over the blown portion of the wing increases compared to the freestream dynamic pressure q_{∞}.
- AR or b: Wing aspect ratio or wingspan, depending on the chosen approach (constant aspect ratio or constant span)

A. Setup

To quickly evaluate each subject a simple mission to simulate it over points of interest was created. Each one was run on a simple three-segment mission that has no real practical meaning. It consists of a level-flight segment at sea-level and at stall speed V_{stall} of 61 kt, using the full-flapped configuration and with the high-lift propellers turned on. Following that a climb segment was created just to connect the first one to a cruise segment at an altitude of 10000 ft and a speed of 168 kt. On these last two segments the aircraft is on its cruise configuration, with the flaps up and high-lift propellers turned off. The analysis mission profile can be seen on Figure 10.

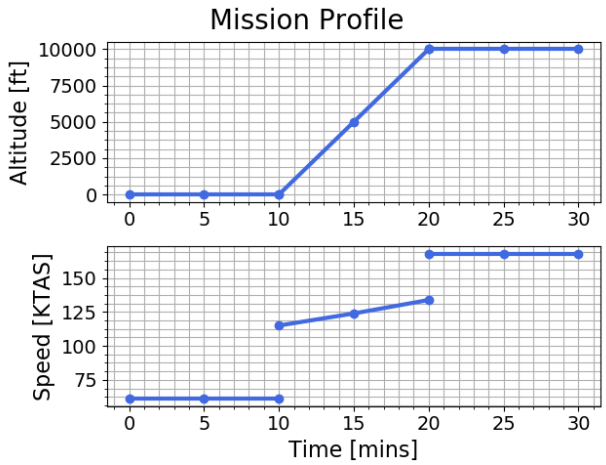

Fig. 10 Analysis mission used to gather data from the subjects.

B. Lift augmentation

The first thing to be analysed was the result of the lift augmentation on all of the subjects. It was seen before that a given dynamic increment does not generate all the lift increase that would be expected on a wing because not all of it is blown and because of slipstream height effects.

Figure 11 shows the result of the lift augmentation on the vertical axis over a range of wing area ratios shown on the horizontal axis. On the constant aspect ratio approach, the lift augmentation for each value of q_{ratio} is practically unchanged with the variation of S_{ratio}, while on the constant wingspan approach the augmentation increases with lower values of wing area ratio. This increase is the effect of the wing chord becoming smaller with the reduction of wing area and, since the propellers radii do not change, the radius-to-chord ratio increases making the lift augmentation more efficient. On the constant aspect ratio approach the propellers radii are reduced along with wing chord so that the ratio does not change and neither does the lift augmentation.

For any given value of S_{ratio} there is a minimum value of lift augmentation that is required so that the aircraft won't stall. This value, which is simply equal to $1/S_{ratio}$, is shown on the figures by the dashed black line. The intersection of this line with each q_{ratio} lift augmentation curve represents the minimum design dynamic pressure ratio required to make a feasible aircraft for a given S_{ratio}, generating the curves shown on Figure 12.

These curves are very important and will be used on all the subsequent analyses because they effectively remove one variable from the system, attributing a value of q_{ratio} to every value of S_{ratio} for a feasible design. This allows to easily verify how all the parameters behave only for the best feasible design since aircraft designed with values of dynamic pressure ratio different from the ones in these curves are either unfeasible or oversized, being then heavier and less efficient.

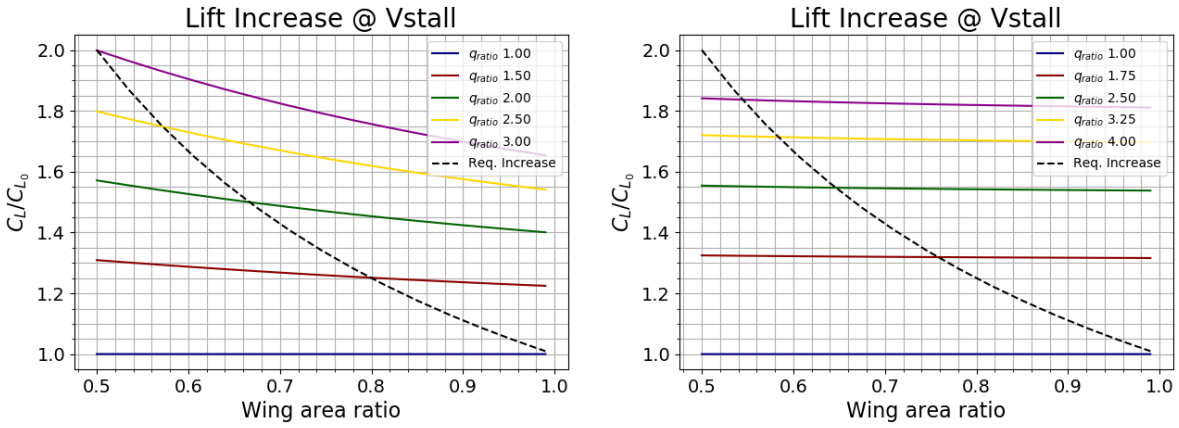

(a) Constant wingspan.

(b) Constant aspect ratio.

Fig. 11 Lift augmentation for various designs.

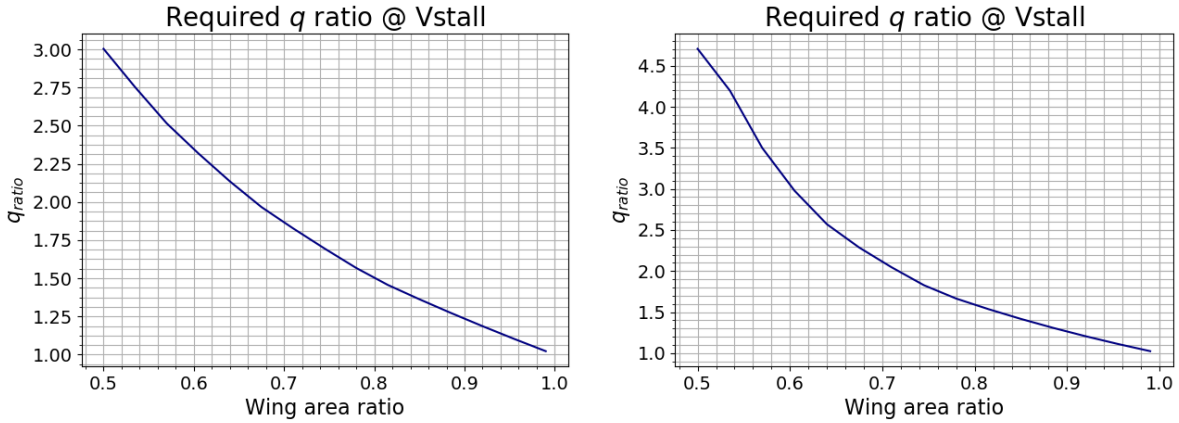

(a) Constant wingspan.

(b) Constant aspect ratio.

Fig. 12 Minimum design q_{ratio} for various values of S_{ratio}.

C. Thrust

The byproduct of lift augmentation through increasing dynamic pressure is the generation of thrust. The increase on the freestream velocity results in the acceleration of air mass, generating thrust as described by the momentum theory. It is important then to evaluate, on the critical flight conditions such as stall, if the designs are feasible or not based on how much thrust is required for lift augmentation. Note that the results shown here are for the stall configuration, with full flaps and high-lift motors powered on.

Figure 13 gives insight on the feasibility of the subjects by comparing the HLP required thrust for the minimum required q_{ratio} against the thrust needed for a level flight at the stall speed of 61 kt. For S_{ratio} values above 0.8 the designs are clearly feasible, since the HLP supply part of the required thrust and the rest can be supplied by the cruise propeller.

For lower values, however, there is a complication because the high-lift propellers generate more thrust than what is needed to maintain flight at stall speed. This at first may not seem like a problem but it means that these aircraft would never be able to decelerate to lower speeds if needed, such as for touchdown. It also means that to fly at such low speeds the HLP would have to generate less thrust, reducing lift and stalling the aircraft, meaning that the effective stall speed for such designs are actually higher than the desired 61 kt.

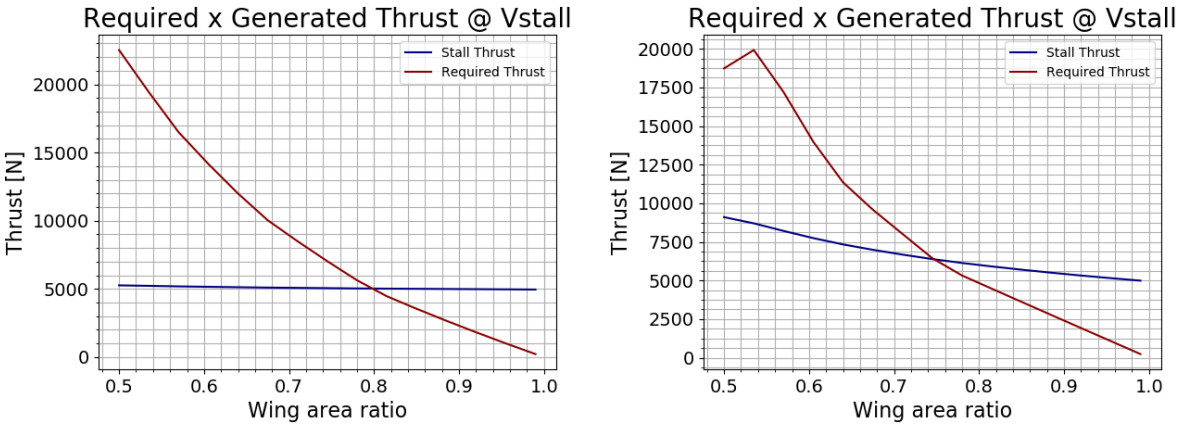

(a) Constant wingspan.

(b) Constant aspect ratio.

Fig. 13 Comparison between HLP thrust and level flight at V_{stall} required thrust.

These results limit the design space by quite a lot. It may be possible to achieve wing area ratios a little smaller than the limits shown on these graphs by increasing drag through new mechanisms on the aircraft like fuselage spoilers, or by adjusting the cruise propeller to create drag and using the generator to direct some of that power to the high-lift propellers. It seems, however, unlikely that the goal of a twofold increase on the wing loading can be achieved

D. Drag and Efficiency

The reduction of wing area affects the total drag of the aircraft, both the parasite drag by reducing the wetted area and adding the nacelles, and the induced drag, by changing aspect ratio and flying at different values of C_L. It is important to notice that the values shown here are for the cruise configuration, where the aircraft is flying with flaps up and the high-lift motors turned off.

On Figure 14 the behavior of the total aircraft drag coefficient is shown in two ways. The solid lines represent the actual drag coefficient for each subject, and is always increasing because once the wing area is reduced so is the aircraft reference area, causing an increase on the drag coefficient. This makes it very hard to compare subjects to each other and the reference, because there is no way of identifying any gains. That brings us to the dashed lines, where the drag coefficients from the solid lines have been normalized against the original aircraft's reference area of 25.96 m^2. By doing this, putting it all on the same basis, it is easier to see what is going on. The normalized drag coefficient is what is used moving forward to understand and compare the subjects.

The drag on the fixed span approach has a very simple behavior, always reducing along with the wing area. On the fixed aspect ratio, though, the behavior is very different, and drag actually increases for lower values of S_{ratio}. To better understand this, a detailed analysis of the parasitic and induced drag is required.

Figure 15 shows the parasitic drag coefficient for each approach, and they both share the same behavior, reducing along with the wing area. Note that for each value of design q_{ratio} the parasitic drag is different because the motors have different power requirements and diameters, generating different values of nacelle drag. The dashed line that represents the minimum feasible design goes from one line to the other as the wing reduces showing the effects of the nacelle drag on the designs.

The induced drag, however, behaves very differently between the two approaches, as can be seen on Figure 16. On both approaches the induced drag for each value of design q_{ratio} is practically on top of each other, which makes sense because the nacelles during cruise should not affect the induced drag. The reason behind the slight differences that can be seen on the constant wingspan graph is due to the higher parasitic drag, which makes the cruise propeller generate more thrust. Because of the angle of attack and aircraft pitch part of this thrust helps with lift generation, so the wing generates less lift and thus the induced drag is reduced. This is also the reason behind slightly lower values of induced drag when wing area is smaller: higher angles of attack mean higher pitches and more upwards thrust, which means less lift on the wing and less induced drag. Despite those minor variations, though, induced drag can be considered constant for the constant wingspan subjects since the differences are so small.

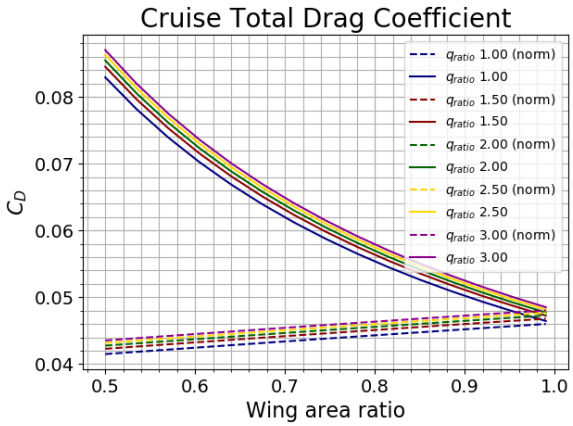

(a) Constant wingspan.

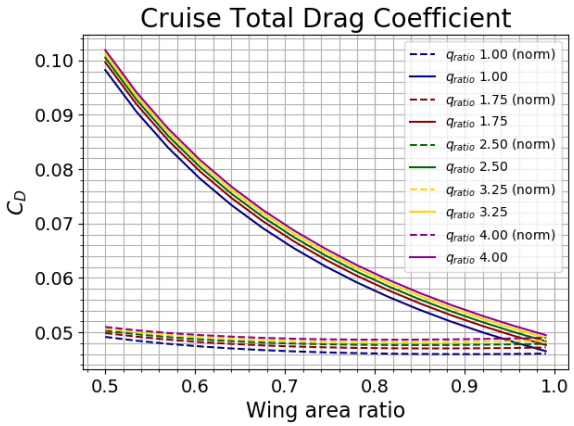

(b) Constant aspect ratio.

Fig. 14 Total aircraft drag coefficient.

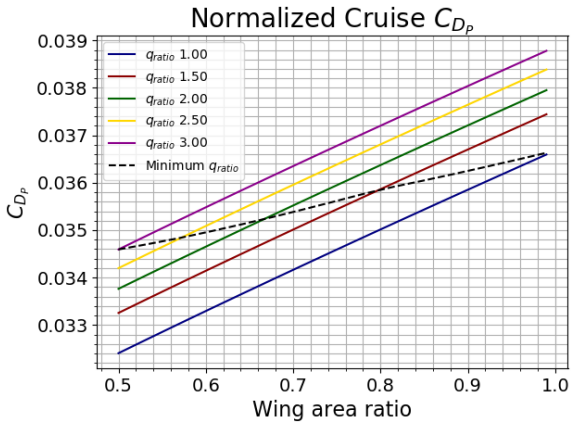

(a) Constant wingspan.

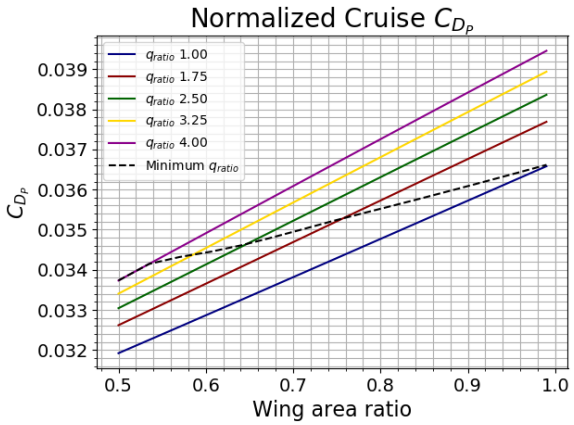

(b) Constant aspect ratio.

Fig. 15 Normalized parasite drag coefficient.

On the constant aspect ratio case, though, the induced drag is greatly increased with the reduction of the wing area. This is due to the fact that, with the same aspect ratio, flying at higher values of C_L inevitably generates more induced drag. This increase does not happen on the constant wingspan approach because as the wing area reduces the aspect ratio increases and the effects of higher C_L are offset by better wing efficiency. On the constant aspect ratio approach, where this does not happen, there is a point where the increase in induced drag offsets any parasitic drag gains by the wing reduction, causing the total aircraft drag to increase as shown in Figure 14.

This brings us to the aerodynamic efficiency of the subjects, which can be seen on Figure 17. It pretty much follows what the total drag behavior dictates. For the constant wingspan approach there is a constant increase of efficiency with the reduction of wing area, while on the constant aspect ratio approach the efficiency starts to degrade after a point due to the increase in induced and total drag. These results show that maintaining the aspect ratio of the wing unchanged as the area is reduced is not the best approach to this problem.

What is really interesting from these results, though, is that even on the constant wingspan approach the aerodynamic gains are not what was expected. The Grand Caravan drag polar showed the potential for an improvement of 23% in aerodynamic efficiency, but the maximum value showed by these graphs is on the order of 4%. If only the feasible design space dictated by the thrust requirements early on this section is considered, the possible gains are even lower.

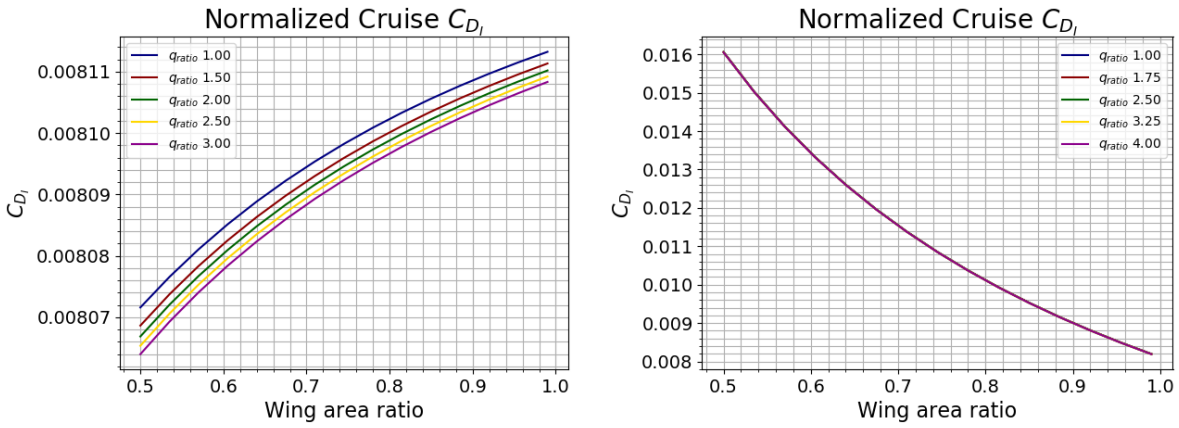

(a) Constant wingspan.

(b) Constant aspect ratio.

Fig. 16 Normalized induced drag coefficient.

Another very interesting point that can be seen from these graphs is that the reason why the expected gains are not reached are not solely because of the drag increase from the nacelles. In fact, the line for a q_{ratio} of 1.0, which is the line for wing area reduction without the addition of propellers and nacelles, shows a maximum gain of approximately 8.5%, also way below the expected 23%.

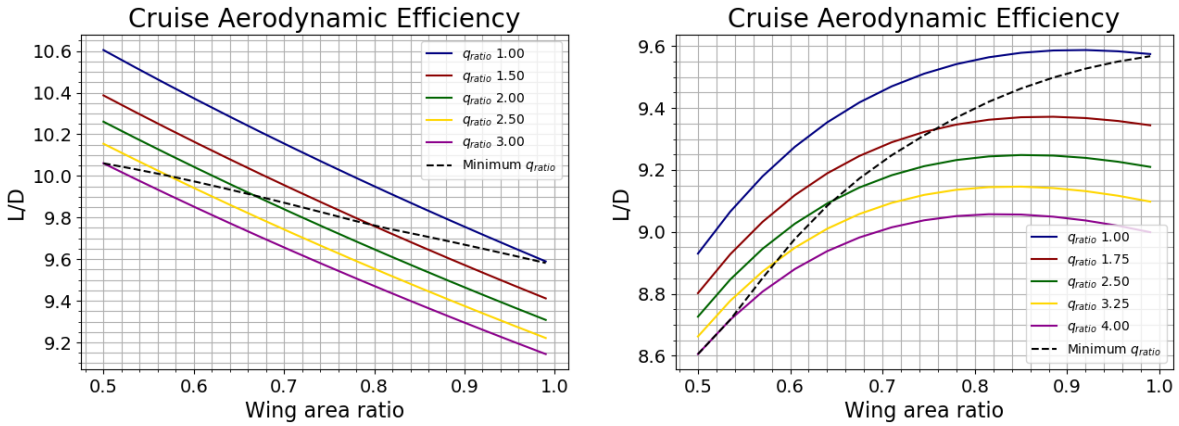

(a) Constant wingspan.

(b) Constant aspect ratio.

Fig. 17 Aerodynamic efficiency.

This leads to the perception that even with the wing area reduction the aircraft are not flying near the peak of the L/D curve. In fact, from the graphs presented so far in this section, it seems that the only actual gains of efficiency come simply from the reduction of wing wetted area and nothing more.

E. Drag Polar

An investigation on the actual drag polar of each subject on the minimum feasible design list was made, running them on the same mission presented on Fig. 5 that was used to calibrate the original aircraft drag polar. As before, the data is fitted to a $C_{D_0} + k\ C_L^2$ curve and the results are seen on Figure 18.

With the reduction of the wing area the value of C_{D_0} is increased, even with the net reduction of parasitic drag, while the value of k decreases due to the aspect ratio increase for the constant wingspan approach. For the constant aspect

ratio approach the value of k should not change in theory but it changes a little bit because it is found based on a fit of data, and other effects like drag change due to the nose propeller slipstream acting on the fuselage are taken into account.

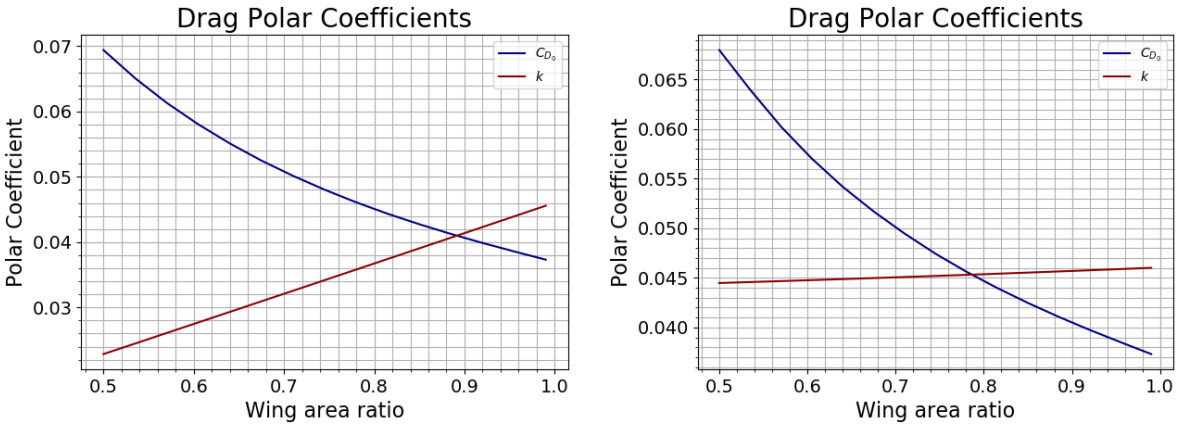

(a) Constant wingspan.

(b) Constant aspect ratio.

Fig. 18 C_{D_0} and k changes.

Figure 19 shows the ratio between the cruise and optimal C_L for both approaches and it can be seen that on the constant aspect ratio case the flight lift coefficient actually gets considerably closer to the optimal value, while for the constant wingspan approach the approach is barely noticeable. It is clear that even though the aircraft fly at higher values of C_L with the reduction of wing area the peak of the L/D curve shifts for even higher numbers in a way that the aircraft will never reach this peak without changing speed or altitude.

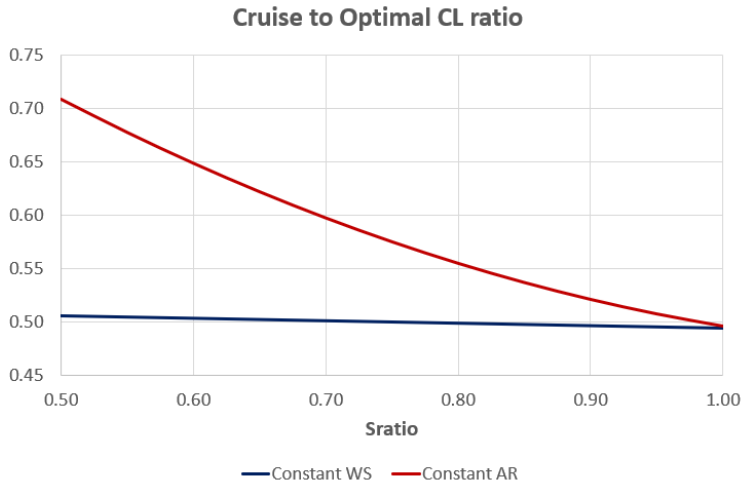

Fig. 19 Ratio between cruise lift coefficient and the optimal value.

These results go against what was proposed by several references and, upon further investigation, it was found that this is due to a very strong assumption made to show the potential of the gains in this technology, which was a constant drag polar assumption. This ends up neglecting the real effects that changing the wing size will actually bring to the aircraft performance and indirectly implies that, by reducing the wing area, the drag of the aircraft as a whole reduces as well when actually only the wing parasitic drag is changed.

To get a better comparison, Figure 20 presents curves of L/D versus cruise speed for both approaches used in this work and for an approach that uses the assumption of a constant drag polar. The thick black line shows the original aircraft, with the peak L/D of roughly 12 happening at around 118 kt. The blue lines show how this curve shifts with

the reduction of wing area if the assumption of a constant drag polar is used and it does in fact shift to higher speeds, meaning that if this was true the proposed gains would have been achieved.

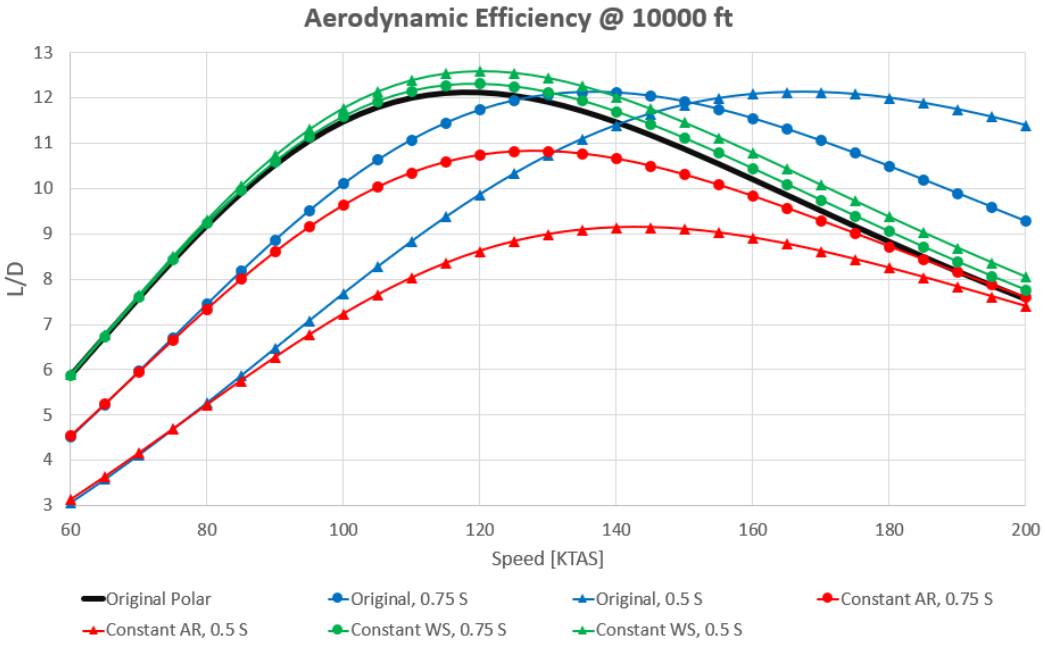

Fig. 20 Behavior of the L/D curve with wing reduction.

The green and red lines show how this curve shifts if this assumption is not made, which is the case in this work, for both the constant wingspan and constant AR approaches, and the results shown by the previously presented graphs can be seen here with ease. For the constant wingspan approach the peak value increases a little bit and shifts slightly to higher speeds while on the constant AR approach the peak shifts considerably to higher speeds but its peak value decreases drastically. It is clear that the assumption of a constant drag polar is quite optimistic, yielding deceivingly positive results for this technology while, when taking into account the changes in the drag polar, the achieved gains are minimal or even non-existent.

VI. Conclusion

A Cessna Grand Caravan model was implemented and modified to include the effects of high-lift propellers through the use of distributed electric propulsion. A broad design space was explored to evaluate the effects of these modifications in thrust, drag and aerodynamic efficiency.

The increase in dynamic pressure by the propellers for lift augmentation purposes showed to generate a lot of thrust, virtually limiting the design space for the aircraft. Drastic wing area reductions proved not to be viable for the aircraft without some sort of drag-increasing mechanism to comply with FAR 23 stall speed requirements.

Regarding aircraft drag, the induced portion is not improved with the reduction of wing area that the distributed propulsion allows. It either stays constant if the wingspan remains constant, or increases if the aspect ratio remains constant while the wing area is reduced. As per parasitic drag, a reduction is seen on both approaches and it can be traced to the reduction in wetted area due to smaller wings. Since wing parasitic drag accounts for just a fraction of aircraft total drag, however, this reduction yielded very modest increases in aerodynamic efficiency that do not match the gains that are proposed by the literature when using the assumption of a constant drag polar. It was shown that reduction in wing area, if not reflected properly on the drag polar coefficients, leads to optimistic results in drag reduction and aerodynamic efficiency increase.

References

[1] Kim, H. D., Perry, A. T., and Ansell, P. J., "A Review of Distributed Electric Propulsion Concepts for Air Vehicle Technology," *AIAA/IEEE Electric Aircraft Technologies Symposium, 2018*, American Institute of Aeronautics and Astronautics, Cincinnati, OH, 2018.

[2] Jansen, R., Bowman, C., Jankovsky, A., Dyson, R., and Felder, J., "Overview of NASA Electrified Aircraft Propulsion (EAP) Research for Large Subsonic Transports," *AIAA/SAE/ASEE Joint Propulsion Conference, 53., 2017*, American Institute of Aeronautics and Astronautics, Atlanta, GA, 2017.

[3] Gesell, H., Wolters, F., and Plohr, M., "System analysis of turbo-electric and hybrid-electric propulsion systems on a regional aircraft," *The Aeronautical Journal*, Vol. 123, No. 1268, 2019, pp. 1602–1617.

[4] Lenssen, R., "Series Hybrid Electric Aircraft," M. sc in aerospace engineering, Delft University of Technology, Delft, 2016.

[5] Dean, T., Wroblewski, G. E., and Ansell, P. J., "Mission Analysis and Component-Level Sensitivity Study of Hybrid-Electric General Aviation Propulsion Systems," *AIAA Aerospace Sciences Meeting, 2018*, American Institute of Aeronautics and Astronautics, Kissimee, FL, 2018.

[6] Pornet, C., and Isikveren, A., "Conceptual design of hybrid-electric transport aircraft," *Progress in Aerospace Sciences*, Vol. 79, 2015, pp. 114–135.

[7] NAS, *Commercial Aircraft Propulsion and Energy Systems Research*, The National Academic Press, Washington, DC, 2016.

[8] Stoll, A. M., Bevirt, J., Moore, M. D., Fredericks, W. J., and Borer, N. K., "Drag Reduction Through Distributed Electric Propulsion," *AIAA Aviation Technology, Integration, and Operations Conference, 14., 2014*, American Institute of Aeronautics and Astronautics, Atlanta, GA, 2014.

[9] Stoll, A. M., "Comparison of CFD and Experimental Results of the LEAPTech Distributed Electric Propulsion Blown Wing," *AIAA Aviation Technology, Integration, and Operations Conference, 15., 2015*, American Institute of Aeronautics and Astronautics, Dallas, TX, 2015.

[10] Stoll, A. M., and Mikic, G. V., "Design Studies of Thin-Haul Commuter Aircraft with Distributed Electric Propulsion," *AIAA Aviation Technology, Integration, and Operations Conference, 16., 2016*, American Institute of Aeronautics and Astronautics, Washington, DC, 2016.

[11] Borer, N. K., Patterson, M. D., Vicken, M. D., Moore, M. D., Clarke, S., Redifer, M. E., Christie, R. J., Stoll, A. M., Dubois, A., Bevirt, J., Gibson, A. R., Foster, T. J., and Osterkamp, P. J., "Design and Performance of the NASA SCEPTOR Distributed Electric Propulsion Flight Demonstrator," *AIAA Aviation Technology, Integration, and Operations Conference, 16., 2016*, American Institute of Aeronautics and Astronautics, Washington, DC, 2016.

[12] Patterson, M. D., "Conceptual Design of High-Lift Propeller Systems for Small Electric Aircraft," Phd in aerospace engineering, Georgia Institute of Technology School of Aerospace Engineering, 2016.

[13] Lukaczyk, T. W., Wendorff, A. D., Colonno, M., Economon, T. D., Alonso, J. J., Orra, T. H., and Ilario, C., "SUAVE," *AIAA/ISSMO Multidisciplinary Analysis and Optimization Conference, 16., 2015*, American Institute of Aeronautics and Astronautics, Dallas, TX, 2015.

[14] Gudmundsson, S., *General aviation aircraft design*, Butterworth-Heinemann, Waltham, MA, 2014.

[15] Gallani, M. A., "Analysis of the Application of Distributed Propulsion on a Turboelectric General Aviation Aircraft," M. eng. in aeronautical engineering, Instituto Tecnológico de Aeronáutica, São José dos Campos, 2019.

[16] *Information manual Grand Caravan*, Cessna Aircraft Company, Wichita, 2008.

[17] L. Ting, C. L., and Kleinstein, G., "Interference of Wing and Multipropellers," *AIAA Journal*, Vol. 10, No. 7, 1972, pp. 906–914.